FirnLearn: A Neural Network based approach to Firn Densification Modeling for Antarctica

Ayobami Ogunmolasuyi[1], Colin Meyer[1], Ian McDowell[2], Megan Thompson-Munson[3], Ian Baker[1]

[1] *Thayer School of Engineering, Dartmouth College, Hanover, NH 03755*

[2] *Graduate Program of Hydrologic Sciences, University of Nevada, Reno, NV 89557*

[3] *University of Colorado, Boulder, CO 80309*

Correspondence: Ayobami Ogunmolasuyi <ayobami.o.ogunmolasuyi.th@dartmouth.edu>

ABSTRACT. Understanding firn densification is essential for interpreting ice core records, predicting ice sheet mass balance, elevation changes, and future sea-level rise. Current models of firn densification on the Antarctic Ice Sheet (AIS) are semi-empirical, complex, and rely on sparse climatic data and surface density observations. In this work, we introduce a deep learning technique to study firn densification on the AIS. Our model, evaluated on six density cores, shows an average root mean square error (RMSE) of 39 kg m^{-3} and explains 98% of the variance (r^2 = 0.98). We use the model to generate surface density and the depths to the 550 kg m^{-3} and 830 kg m^{-3} density horizons across the AIS to assess spatial variability. Comparisons with observations and the Herron and Langway (1980) model at six locations with different climate conditions demonstrate that FirnLearn more accurately predicts density profiles in the second stage of densification and complete density profiles without direct surface density observations. This work establishes deep learning as a promising tool for understanding firn processes and advancing a more universally applicable firn model.

INTRODUCTION

As snow falls on the surface of the Antarctic Ice Sheet (AIS), it compacts into glacial ice, transitioning through an intermediate stage called firn. Firn has a density that ranges between that of snow (350 kg m^{-3}) and glacial ice (917 kg m^{-3}) depending on the network of interconnected pores which exchange air with the atmosphere (Buizer, 2013; Van den Broeke, 2008). Firn densification into glacial ice is controlled by, for example, temperature, accumulation rate, grain size, wind, impurity concentration, and water content. Understanding firn densification is important as it affects several processes in ice sheets. Firstly, given that densification changes in response to climatic factors, it causes uncertainty in ice-sheet elevation and mass balance estimates (Helsen and others, 2008; Smith and others, 2020). Secondly, densification results in the closure of the interconnected network of pores, which when closed off, traps gases in the ice. The age difference between the trapped gases and the ice is important for interpreting ice core records (Alley, 2000; Cuffey and Paterson, 2010). Lastly, the pore space within firn columns serves as storage for meltwater from the warming climate, hence, breaking the link between surface melt, runoff, and sea-level rise Harper and others (2012); Forster and others (2013); Meyer and Hewitt (2017). Consequently, a comprehensive understanding of firn processes is crucial for accurately predicting ice sheet responses to climate change The-Firn-Symposium-Team (2024).

Firn densification is controlled by microstructural evolution (Anderson and Benson, 1963; Arnaud and others, 2000). It occurs in three stages, each characterized by distinct mechanisms. Initially, grain boundary sliding, vapor transport, and surface diffusion dominate until reaching a density of 550 kg m^{-3} (Anderson and Benson, 1963; Alley, 1987; Gow, 1969; Maeno and Ebinuma, 1983). In the second stage, pore space reduction limits vapor diffusion, giving way for sintering processes and recrystallization until a density of 830 kg m^{-3} is attained (Gow, 1969; Maeno and Ebinuma, 1983). The depth at 830 kg m^{-3} is typically denoted the pore close-off depth. Finally, at the firn-ice transition, bubble shrinkage and compression become dominant until the density of ice (917 kg m^{-3}) is reached (Bader, 1965). Several studies have been aimed at shedding more light on the microstructural processes in firn (Maeno and Ebinuma, 1983; Freitag and others, 2004; Kipfstuhl and others, 2009; Lomonaco and others, 2011; Burr and others, 2018; Li and Baker, 2021; Ogunmolasuyi and others, 2023). However, a comprehensive understanding of large-scale implications of firn densification requires an integration between the underlying microphysics and modeling. To this end, over four decades of effort has been undertaken to develop firn densification models

(Herron and Langway, 1980; Alley, 1987; Barnola and others, 1991; Arnaud and others, 2000; Kaspers and others, 2004; Ligtenberg and others, 2011; Morris and Wingham, 2014; Stevens and others, 2020; Meyer and others, 2020; Stevens and others, 2023). These models are either empirical (Herron and Langway, 1980; Barnola and others, 1991; Li and Zwally, 2011) or microphysics-based (Alley, 1987; Arnaud and others, 2000; Morris and Wingham, 2014).

However, due to an incomplete understanding of the underlying physics of firn densification, the microphysics approaches do not match observations. Hence, most firn densification models are empirical, predicting density evolution based only on the accumulation rate and temperature. These variables are usually obtained from ice core data such as (Buizert and others, 2012), regional climate models such as the Regional Atmospheric Climate (RACMO) (Noël and others, 2018) or the most accurate sources, long-term weather station data such as the Greenland climate network (GCN) (Steffen and Box, 2001). These models are then used to fit depth-density profiles derived from firn cores, with an assumption that the accumulation rate, surface density and the firn column are in steady state known as Sorge's law (Bader, 1954). While these models have served the glaciology community reasonably well, they do not describe the physics of firn densification and therefore do not have much predictive power. These empirical models also have several uncertainties in the inputs, i.e. the atmospheric forcing and model parameters (LUNDIN and others, 2017; Verjans and others, 2020).

In this study, we explore a novel approach to firn densification modeling based on a statistical analysis of known depth-density profiles as an attempt to improve the firn density estimates of empirical models. We use comparisons with the (Herron and Langway, 1980) model, denoted HL, as a case study. In recent years, the utility and significance of machine learning methods have grown. In particular, the ever-growing volume of data combined with hardware and optimization algorithms that allow complex systems to be fitted effortlessly has resulted in advances across various scientific fields, including earth sciences (Camps-Valls and others, 2020; Reichstein and others, 2019), among several other applications. While machine learning techniques, particularly artificial neural networks (ANNs) have seen increasing application in glaciology, including for simulating glacier length (Steiner and others, 2005; Nussbaumer and others, 2012), and modeling glacier flow, evolution and mass balance (Bolibar and others, 2020; Brinkerhoff and others, 2021), less attention has been paid to its implementation in firn densification modeling. Only a few machine learning models have been applied to firn processes. Rizzoli and others (2017) applied clustering techniques to characterize snow facies while Dell and others (2022) used a combination of clustering and classification techniques to identify slush and melt-pond water and Dunmire and others (2021) employed a convolutional neural network to detect buried lakes across the GrIS. Notably, the only studies that have applied machine learning methods to modeling firn density was done by Li and others (2023), who trained a random forest on radiometer and scatterometer data to derive spatial and temporal variations in Antarctic firn density, and Dunmire and others (2024) who used a random forest to predict ice-shelf effective firn air content.

Here, we present a new steady state densification model: FirnLearn, which takes a deep learning approach to firn densification modeling. FirnLearn simulates the evolution of firn density using a deep ANN, fed by density observations from the Surface Mass Balance and Snow on Sea Ice Working Group (SUMup) dataset (Montgomery and others, 2018), and accumulation rate and temperature data from RACMO (Van Wessem and others, 2014; Noël and others, 2018).

In the next section, we present an overview of the data, brief descriptions of the ANN architecture as well as the evaluation techniques used in this study. In section 3, we present applications of FirnLearn to predicting surface density, depths at 550 kg m^{-3} and 830 kg m^{-3} density horizons, as well as firn air content (FAC). Here, we also discuss the performance of FirnLearn in comparison to the depth-density model of Herron and Langway (1980). FirnLearn maintains a high accuracy and it is robust to outliers, changing climatic conditions, as well as surface density data. FirnLearn can also aid in better constraining the physics governing firn densification.

METHODS

DATA

The dataset used in this study is based on field observations and model outputs, extracted from the SUMup dataset Montgomery and others (2018) and RACMO (Van Wessem and others, 2014; Noël and others, 2018) (see figure 1). We combined firn density observations from 1023 locations across the AIS from SUMup with accumulation rate and temperature outputs from RACMO2.3. Given that FirnLearn is a steady-state model, it relies on time-averaged accumulation rate and temperature data, hence we extracted the 1979-2016 average accumulation rate and temperature values from RACMO.

Surface density and depth

The snow/firn density subdataset comes from SUMup. It contains over 2 million unique measurements of density at different depths across both the Antarctic and Greenland Ice Sheets. These density measurements

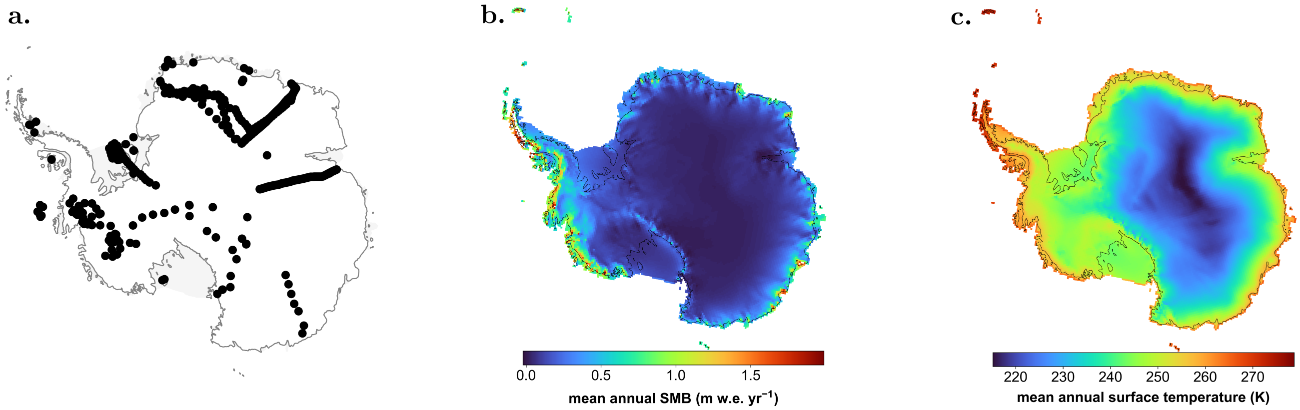

Fig. 1. (a) Locations of the 1023 cores used for density predictions (b)surface mass balance and (c) surface temperature from RACMO2.3

were obtained using density cutters of different sizes used in snow pits, gravitational methods on ice core sections, neutron-density methods in boreholes, X-ray microfocus computer tomography on snow samples, gamma-ray attenuation in boreholes, pycnometers on snow samples, optical televiewer (OPTV) borehole lagging, and density and conductivity permittivity (DECOMP) (Montgomery and others, 2018).

Climate Variables

Accumulation rate: The accumulation rate dataset was obtained from the output of the RACMO2.3 model, containing total precipitation (snowfall and rainfall), runoff, melt, refreezing, and retention. For our accumulation rate input, we average annual surface mass balance (SMB) outputs from RACMO2.3 for 1979-2016. SMB values were converted to meters of water equivalent per year (m w.e. yr^{-1}). For the purpose of this study we assume zero ablation in Antarctica and use SMB as the accumulation rate.

Temperature: For our surface temperature input, we average annual surface temperature outputs from RACMO2.3 for 1979-2016. A combined dataset of Antarctic observations containing latitude, longitude, density, depth, accumulation rate, and temperature was created. Figure 1 shows the location of all the density measurements used in this study

FirnLearn model development

In this section, we describe the procedures for preprocessing the input data, and building, training, validating and testing the machine learning models. In the supplement of this paper, we describe other models employed in predicting density profiles.

Training and testing

After the comprehensive dataset is extracted, we split it into training, testing, and validation sets. We removed 6 cores across the ice sheets to test our model's performance with depth. We selected these sites to be representative of the full spread of regions in Antarctica, selecting one site from the Antarctic Peninsula, East Antarctica, West Antarctica, the South Pole and near the Ross Sea. This also let us test a range of surface density values from around 320 kg m^{-3} to greater than 550 kg m^{-3}. Our tests were conducted on cores from the Larsen C Ice Shelf (66.58 °S,63.21 °W), Marie Byrd Land (78.12°S, 95.65°W), Taylor dome (77.88°S, 158.46°E), near Vostok station (82.08°S, 101.97°E), and two cores from the South Pole [(88.51°S, 178.53°E), (90°S)]. While training the model, we used an 80–20 holdout cross-validation technique to evaluate the skill of our trained model before it was tested. To do this, we removed 20% of the remaining 1018 locations from the training set and the model was then trained on the remaining locations. The splitting procedure is conducted such that there is an equal representation of data from all cores across Antarctica.

Neural network architecture

Artificial Neural Networks (ANNs) are nonlinear statistical models that recognize relationships and patterns between the input and output variables of structured data in a manner that models the biological neurons of the human brain (Hatie and others, 2009; O'Shea and Nash, 2015). The structure of an ANN consists of (1) an architecture of node layers containing the input layer that receives the data, the output layer that produces an estimate of the dependent variable, and hidden layers that take in and sum the weighted inputs and produce an output for other hidden layers or the output layer, (2) an optimization algorithm that determines and updates the weights of the connections between the neurons O'Shea and Nash (2015), and (3) an activation function that determines the output of each neuron.

The goal of the training process is to continuously update the weights in every iteration to minimize a loss function, which in most cases, as in our case, is the mean squared error. This cost function is expressed as

$$min \frac{1}{N} \sum_{i}^{N} (\rho_{NN}(x_i \theta) - \rho_{true}(x_i))^2. \quad (1)$$

The variables that determine the structure and performance of a model are called hyperparameters and they include the number of neurons per layer, number of layers, activation function, optimizer, learning rate, batch size and number of epochs. The hyperparameters used to construct the ANN are tuned using cross validation to find the best performing combination of hyperparameters. FirnLearn, shown in Figure 2 is a seven-layered ANN that consists of 1 input layer with 3 neurons corresponding to the number of selected features, 5 hidden layers with 50, 40, 20, 10, 5 neurons, respectively, and 1 output layer. Leaky ReLUs was chosen as the activation function for the hidden layers. ReLU, short for Rectified Linear Unit, is a piecewise function that outputs the input value if it is greater than 0. It is given by

$$f(x) = \left\{ \begin{array}{ll} 0, & \text{if } x < 0 \\ x, & \text{if } x \geqslant 1 \end{array} \right\}. \quad (2)$$

For the output layer, the sigmoid function was chosen as the activation function. It is represented as

$$f(x) = \frac{1}{1 + e^{-x}}. \quad (3)$$

We used the Adam optimizer technique (Kingma and Ba, 2017) to optimize the weights for gradient descent. We also tuned the learning rate, which determines how much the weights are changed in each iteration. The best performing learning rate was 0.0001 among a starting range of 0.01,0.001 and 0.0001. This learning rate

Herron and Langway, 1980

Herron and Langway (1980), denoted HL in this study, is a widely used semi-empirical firn densification model, upon which many contemporary models are built due to its foundational assumptions. The assumptions made in HL are: (1) the densification rate is a function of the porosity, and (2) the densification rate has an Arrhenius dependence on the temperature. These assumptions are combined to form the equation

$$\frac{d\rho}{dt} = C(\rho_{ice} - \rho), \quad (4)$$

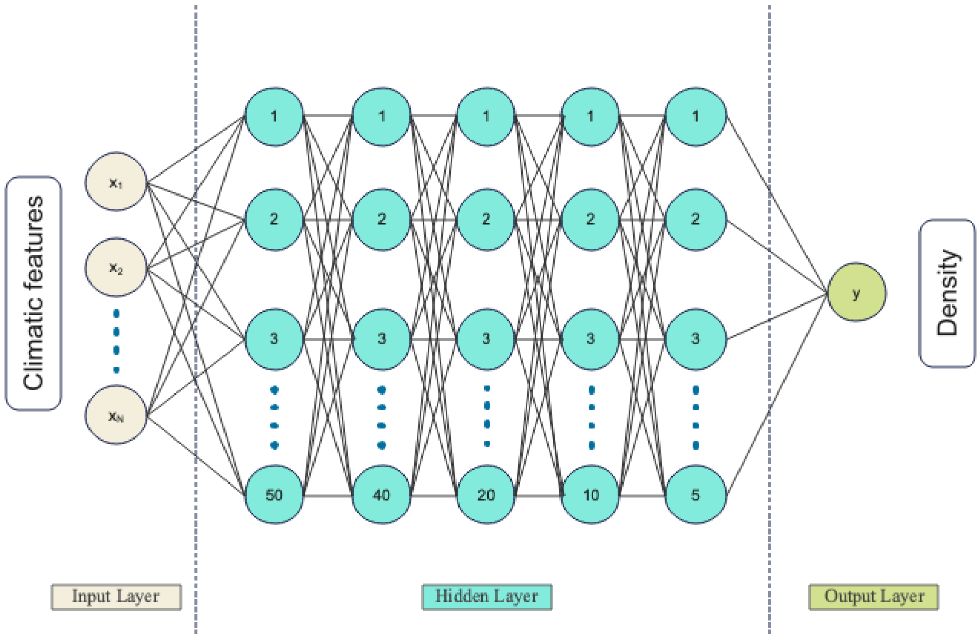

Fig. 2. Artificial Neural Network Architecture

where ρ_{ice} is the density of ice (917 kg m^{-3}), ρ is the density at a given depth, and

$$C = k \exp\left(-\frac{Q}{RT}\right) A^{a}, \tag{5}$$

where k in equation 5 is a temperature-dependent Arrhenius-type rate constant, a is a constant dependent on the densification mechanism, Q is the Arrhenius activation energy (kJ mol^{-1}), R is the gas constant (8.314 kJ mol^{-1} K^{-1}), and T is the mean annual temperature at the site (K). For $\rho \leqslant 550$ kg m^{-3}, we have

$$C = 11 \exp\left(-\frac{10.16}{RT} A\right), \tag{6}$$

and for $\rho > 550$ kg m^{-3}, we have

$$C = 575 \exp\left(-\frac{21.4}{RT} A^{0.5}\right). \tag{7}$$

HL requires a surface density boundary condition. In order to obtain predictions for depth-density profiles, we used both surface density values from observations, as well as surface density predictions from Ligtenberg and others (2011). However, for predicting depths at 550 kg m^{-3} and 830 kg m^{-3}, we used surface density predictions from FirnLearn, which allowed for a direct comparison.

Evaluation

We evaluate our model's performance using several metrics. We use the coefficient of determination r^2 to quantify how well the model predicts the dependent variable (density). It is given by

$$r^2 = 1 - \frac{\sum (y_i - \hat{y}_i)^2}{\sum (y_i - \bar{y})^2}. \tag{8}$$

The root mean squared error (RMSE) is an average measure of the difference between the observed density and the predicted density, given by

$$\text{RMSE} = \sqrt{\frac{\sum_{i=1}^{N} (y_i - \hat{y}_i)^2}{N}}, \tag{9}$$

where N is the number of model-observation pairs, y_i is the true density value, $\hat{y}_i$ is the predicted density value, and $\bar{y}_i$ is the mean of the observed density values. We evaluate the RMSE for an independent test set with a split discussed in the 'Training and testing' section. To estimate the difference between modeled and observed surface density and FAC, we use the relative bias metric. The relative bias is given as

$$\text{relative bias} = \frac{\text{model} - \text{observed}}{\text{observed}} \times 100\%. \tag{10}$$

A positive relative bias indicates an overestimation by the model, while negative bias indicates an underestimation by the model.

RESULTS AND DISCUSSION

Depth-density profiles

We use FirnLearn and HL to simulate firn profiles at the 6 test sites and compare the results in figure 3 . This allows us to visually evaluate the difference in performance between HL and FirnLearn. For HL, we evaluated the HL function using two different surface density values, and the two curves are named HL80-observation and HL80-Ligtenberg. For the HL80-observation curves, we use the surface density value directly from the observations, while for the HL80-Ligtenberg curves, we set the surface density values to predictions from Lightenberg and others (2011). The FirnLearn curves, depicted as black lines, are generated by applying function evaluations of the FirnLearn model, taking in specified accumulation rates, temperatures, and depths, i.e. $\rho = f(A, T, z)$. Of the three models plotted for each core, HL80-observation performs the best, especially in the first stage of densification in figures c, e and f. However, for those cores, FirnLearn outperforms both HL80-observation and HL80-Ligtenberg in the second stage of densification, more especially outperforming HL80-Ligtenberg over the full depth range in three instances (b, c, and f) and demonstrates comparable performance in the remaining three (a , d,and e). In all these curves, the surface density from FirnLearn agrees with the surface density predictions from Lightenberg and others (2011). This explains the similarity observed between FirnLearn's and HL80-Ligtenberg's density profiles.

A more pronounced discrepancy in performance is evident in figure 3a for the Larsen C ice shelf. Here, HL80-observation predicts the density trend with greater accuracy than HL80-Ligtenberg and FirnLearn. Although FirnLearn underperfoms due to an underestimate of the surface density, it accurately predicts the transition to the third stage of densification (densities exceeding 830 kg m^{-3}). In this respect, FirnLearn outperforms HL80-Ligtenberg, which has a more accurate surface density estimate. As discussed in the introduction and evidenced in the SumUp density dataset, surface density measurements have only been collected for a small percentage of the AIS. Figure 3 shows that in the absence of accurate surface density observations, FirnLearn is a better density prediction model than Herron and Langway (1980). This performance demonstrates FirnLearn's effectiveness in firn density prediction.

In Figures 3a, c and e, HL80-Ligtenberg and FirnLearn underestimate the surface density predictions compared to observations, leading to a disagreement with observations in the first stage of densification, however, the predictions from both models for the second stage are in better agreement with observations than HL80-observation. It is worth highlighting that FirnLearn offers the added advantage of providing density information at specific depths for a given site without requiring surface density or density data from previous depths. This characteristic further enhances the speed and utility of FirnLearn in densification research. Additionally, it could be useful in ice core drilling operations for optimized site selection and resource allocation.

Surface Density

We predict surface density across the AIS by putting accumulation rate and temperature from RACMO2.3 (Noël and others, 2018) at $z = 0$ into the trained and validated FirnLearn model. These predictions are based on the equation $\rho = f(A, T, 0)$, where the function f is FirnLearn, A represents the accumulation rate, and T represents the temperature. Across Antarctica, the surface density exhibits a notable spatial

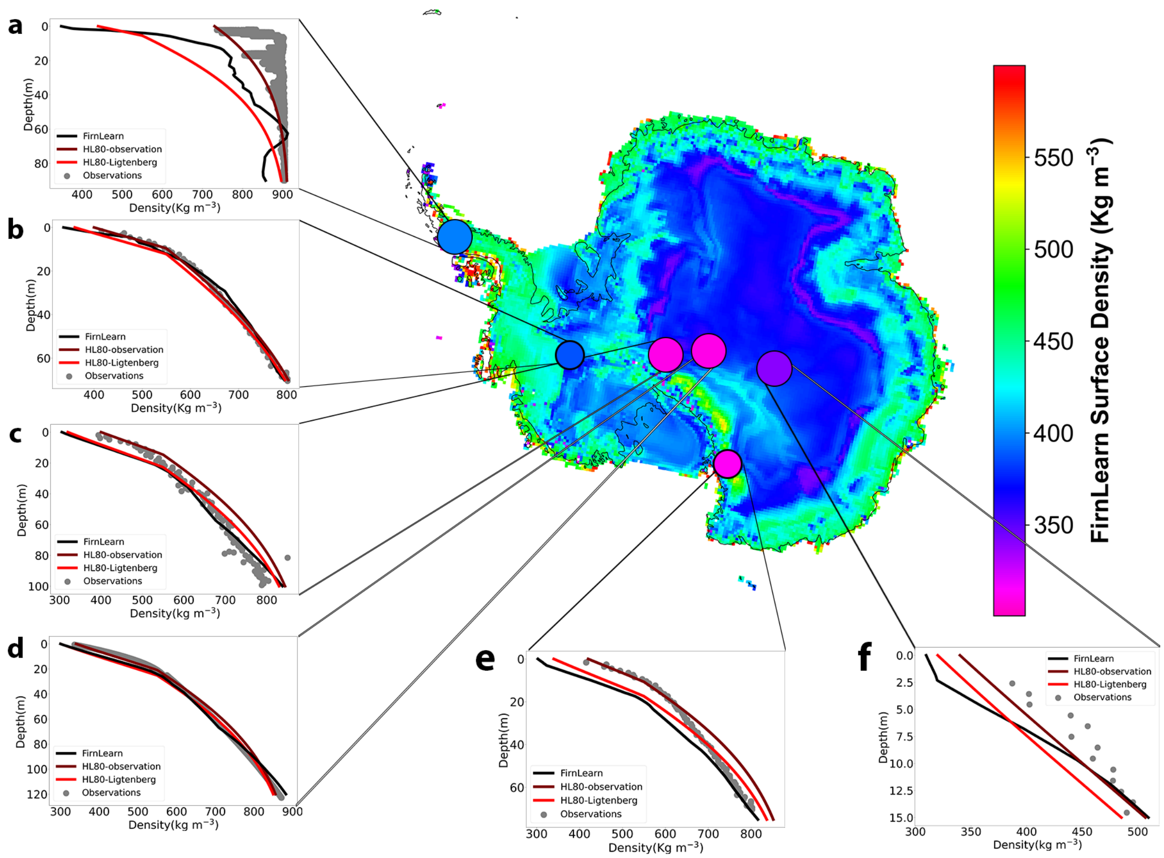

Fig. 3. Depth-density profiles at the 6 test sites. Shown corresponding to each site are the observed density profile in grey, the FirnLearn modeled density in red, and the HL modeled density in black for (a) a location on the Larsen C Ice Shelf, (b) location on the Marie Byrd Land, (c) location near the South Pole,(d) the South Pole, (e) the Taylor dome, and (f) a location near Vostok station

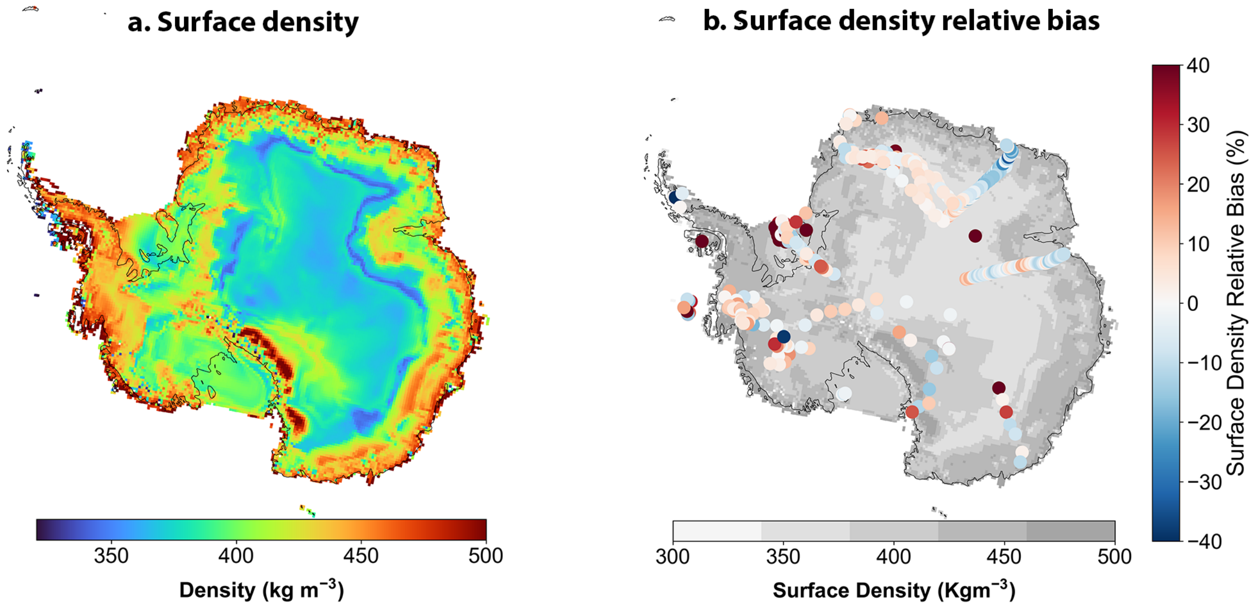

Fig. 4. (a) The predicted surface density field for Antarctica and (b) Relative bias between the predicted surface density and the observed surface density

variation (Figure 4a). In the interior of East Antarctic, we observe relatively lower values in the range 320–380 kg m^{-3}, reflecting the region's colder surface temperatures. In contrast, we find higher surface density values, exceeding 450 kg m^{-3},along the coastal areas and on ice shelves. We attribute these higher densities to the higher temperatures, higher accumulation rates, and the higher wind speeds prevalent in these regions (McDowell and others, 2020). For the majority of the sites, the relative bias is within ±25%, with only one site having a relative bias above 100% (Figure 4b). For this site in the Southeastern Antarctica, FirnLearn overpredicts the surface density by 174%.

Semi-empirical models require a prescribed surface density boundary condition, making these surface density predictions a key output of FirnLearn. The importance of the surface density boundary condition was underscored by Thompson-Munson and others (2023). They employed two models, the physics-based SNOWPACK Bartelt and Lehning (2002) with a surface density that varies based on atmospheric conditions, and the Community Firn Model configured with a semi- empirical densification equation (CFM-GSFC; Stevens and others (2020)) run with a constant surface density of 350 kg m^{-3}. Their analysis of firn properties across the GrIS revealed that SNOWPACK simulated more variability between firn layers compared to CFM-GSFC. The surface density predictions from FirnLearn show low values in the interior (320-380 kg m^{-3}), and higher values (>450 kg m^{-3}) towards the coast and on ice shelves. Importantly, our predictions align with prior research findings (Kaspers and others, 2004; van den Broeke, 2008; Ligtenberg and others, 2011) that have employed parameterizations based on combinations of surface temperature, accumulation rate, wind speed to derive surface density predictions.

Depths at 550 kg m^{-3} and 830 kg m^{-3}

Figure 5a depicts the depth at 550 kg m^{-3} with a depth range from 0-45 m, with higher values (25-45 m) concentrated in East Antarctica and lower values (0-15 m) prevalent in West Antarctica and along the coast. A key trend worth noting is the similarity in patterns between the surface density and z_{550}, with values reducing with a strong gradient from the coast to the interior. Meanwhile, Figure 5c shows a depth range from 20 - 150 m, with higher values (120 - 150 m) predominantly found in East Antarctica. The spatial distribution of z_{830} is different than z_{550} in that for z_{830}, there are higher values in regions of West Antarctica, the Antarctic Peninsula, and certain coastal areas. This is primarily attributed to the higher accumulation rates, which result in the rapid burial of fresh snow. Consequently, a distinct pattern emerges where deeper layers don't densify as much as might be expected. These trends align with the trends observed in earlier models such as van den Broeke (2008) and Lightenberg and others (2011). However, it is important to note a discrepancy between FirnLearn and these studies: the depth at 550 kg m^{-3} mirrors variations in the surface density in a way that it doesn't in FirnLearn. This discrepancy is a potential indicator that in FirnLearn, z_{550} is more a function of densification rate than surface density. In the vicinity of the major ice shelves, such as the Ross, Filchner-Ronne, Larsen and Amery Ice Shelves , z_{550} ranges from 9 to 13 m in FirnLearn, a close range to both van den Broeke (2008) and Lightenberg and others (2011), while z_{830} ranges from 60 to 90 m in FirnLearn, 50 to 70m in van den Broeke (2008) and Lightenberg and others (2011). The discrepancy in z_{830} values may stem from limited data availability at these depths. Figure 5b compares the observed and modelled z_{550} and z_{830} for 120 locations with densities beyond 550 kg m^{-3}, while 5d compares the observed and modelled z_{830} for 39 locations with densities beyond 830 kg m^{-3}. For z_{550}, there is a strong cluster around the line of perfect agreement, especially around mid-range observed depth values (5-15 m). However, at depths below 5 m, there are more points lying above the upper confidence interval for both FirnLearn and HL, indicating that both models typically overestimate the depth values. This is possibly due to an underestimation of surface density, causing the models to densify slower than in observations. At higher depth values, FirnLearn performs better than HL with more HL values lying below the line of perfect agreement. For z_{830}, there is a similar trend with more points above the upper confidence interval for lower observed depth values (0-40 m), and a cluster around

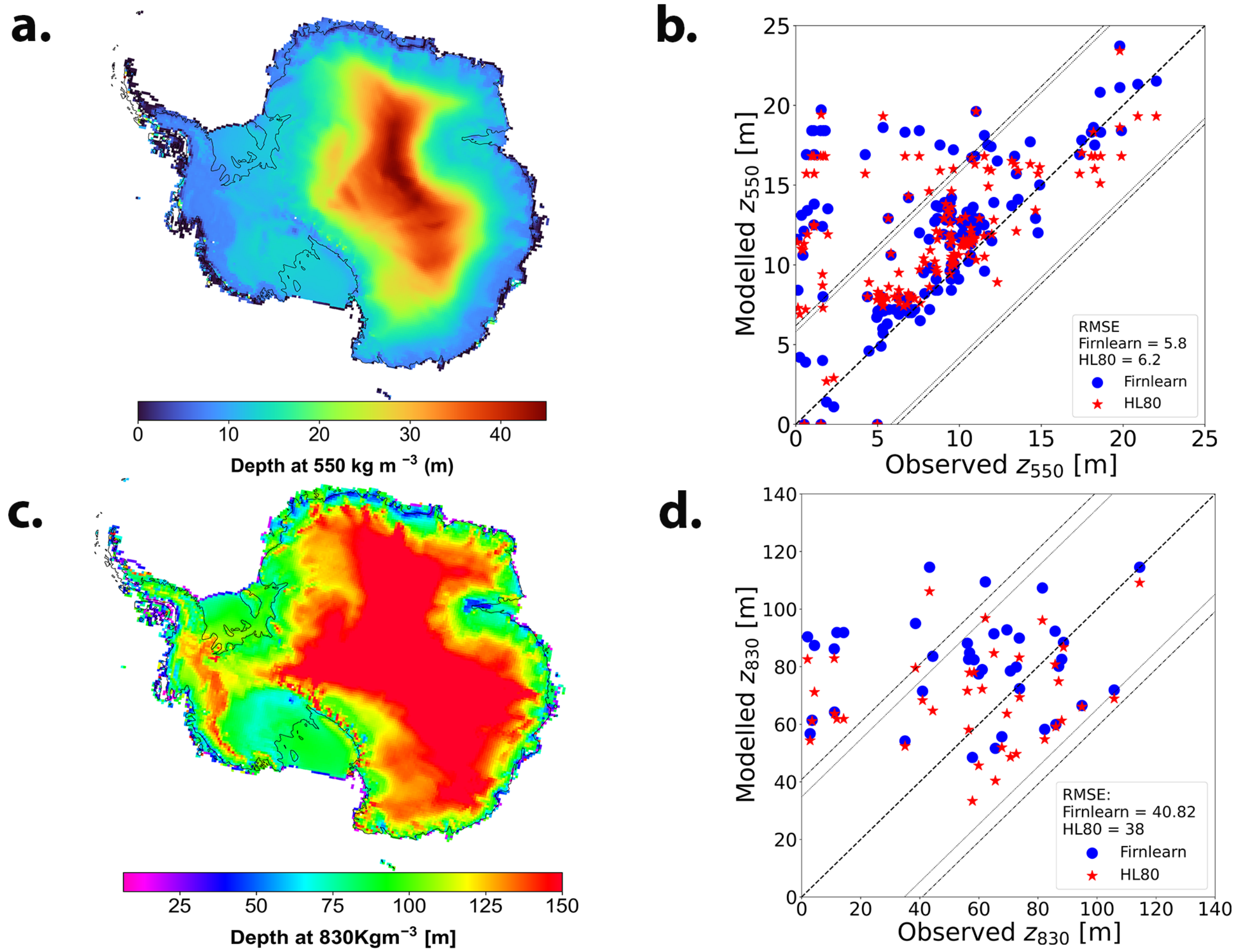

Fig. 5. (a) The predicted depth at 550 kg m^{-3} in meters (b) Comparison of modelled to observed depth at 550 kg m^{-3} (c) The predicted depth at 830 kg m^{-3} in meters (d) Comparison of modelled to observed depth at 830 kg m^{-3}. Here the FirnLearn computed surface density is used for the Herron and Langway (1980) model.

the line of perfect agreement for the remaining points. FirnLearn typically overpredicts z_{830} as compared to HL, which as mentioned earlier may be a result of the sparsity of data at deeper depths.

Firn Air Content

We explore predictions of firn air content (FAC), the amount of air-filled pore space within the firn layer using FirnLearn and HL, and compared them to the FAC from observations. FAC is an important parameter as it improves our understanding and estimates of climate records and gas exchange dynamics as well as representing the amount of meltwater that can be stored within the pore space. To facilitate comparison between FirnLearn and HL, we employed the surface density predictions generated by FirnLearn as the surface density conditions for HL. The FAC is calculated by integrating porosity over the depth of the firn column and is represented as:

$$\text{FAC} = \int_{z_l}^{z_u} \frac{\rho_{ice} - \rho(z)}{\rho_{ice}} dz \tag{11}$$

where ρ_{ice} is the density of ice (917 kg m^{-3}) and $\rho(z)$ is the firn density at a given depth, and the depth interval is set by an upper bound depth z_u and a lower bound depth $z_l = 0$, representing the surface.

As depicted in figure 6a, the majority of density cores used in this study are shallow, indicating correspondingly low observed FAC values in figure 6b. Hence, for a direct comparison between the modeled (FirnLearn and HL), and observed FAC, we evaluated the FAC of each core up to its respective maximum depth from SUMup. This results in the difference in FirnLearn's and HL's evaluation of FAC being a reflection of their accuracy in predicting the densities in the first stage of densification. Very little difference is visually observed between the observed FAC and FirnLearn's and HL's predicted FAC (Figures 6 b, c and d). Figures 6 e and f depict the relative bias between FirnLearn's FAC and the observed FAC, and between HL's FAC and the observed FAC respectively. Given that we used FirnLearn's surface density as the boundary condition for HL's FAC calculations, FirnLearn's FAC bias values are similar to HL's FAC bias values, with a bulk relative bias of -5.5% for HL and -5.7% for FirnLearn. The root mean squared error however, shows a better performance in FirnLearn than in HL. In west Antarctica where we have deeper cores, more variation is observed. Specifically, FirnLearn slightly overestimates FAC in these deeper cores, while HL slightly underestimates FAC. To obtain a better representation of the full firn column, we recalculated FAC, using FirnLearn and HL across a wider accumulation rate (0-6 m.w.e.yr $^{-1}$) and temperature (215-270 K [-58 – -3°C]) space from the surface to 100 m depth. The heat maps shown in figure 7 depict the firn air content from FirnLearn, Herron and Langway (1980), and the difference between the two. As shown in these figures, FirnLearn and HL produce similar FAC patterns, with FAC being highest at high accumulation rates and low temperatures, and lowest at low accumulation rates and high temperatures. Relating this to ice sheets, FAC is predicted by both models to be approximately 30 - 50 m on the interior, where accumulation rates and temperatures are low (<1 m.w.e yr^{-1} and <220 K [-53°C] respectively), and in coastal regions where accumulation rates could be higher than 5 m.w.e yr^{-1}, and temperatures could be higher than 250 K [-23°C]. In West Antarctica, with accumulation rates between 2 and 5 m.w.e yr^{-1}, and temperatures between 235 and 250K, FAC is predicted by FirnLearn to be greater than 70 m, and predicted by HL to be 45-50 m.

Figure 7c shows that on average FAC is greater in FirnLearn than in HL, except within the low accumulation rate and cold temperature regime, where FAC is less in FirnLearn than in HL. The regions

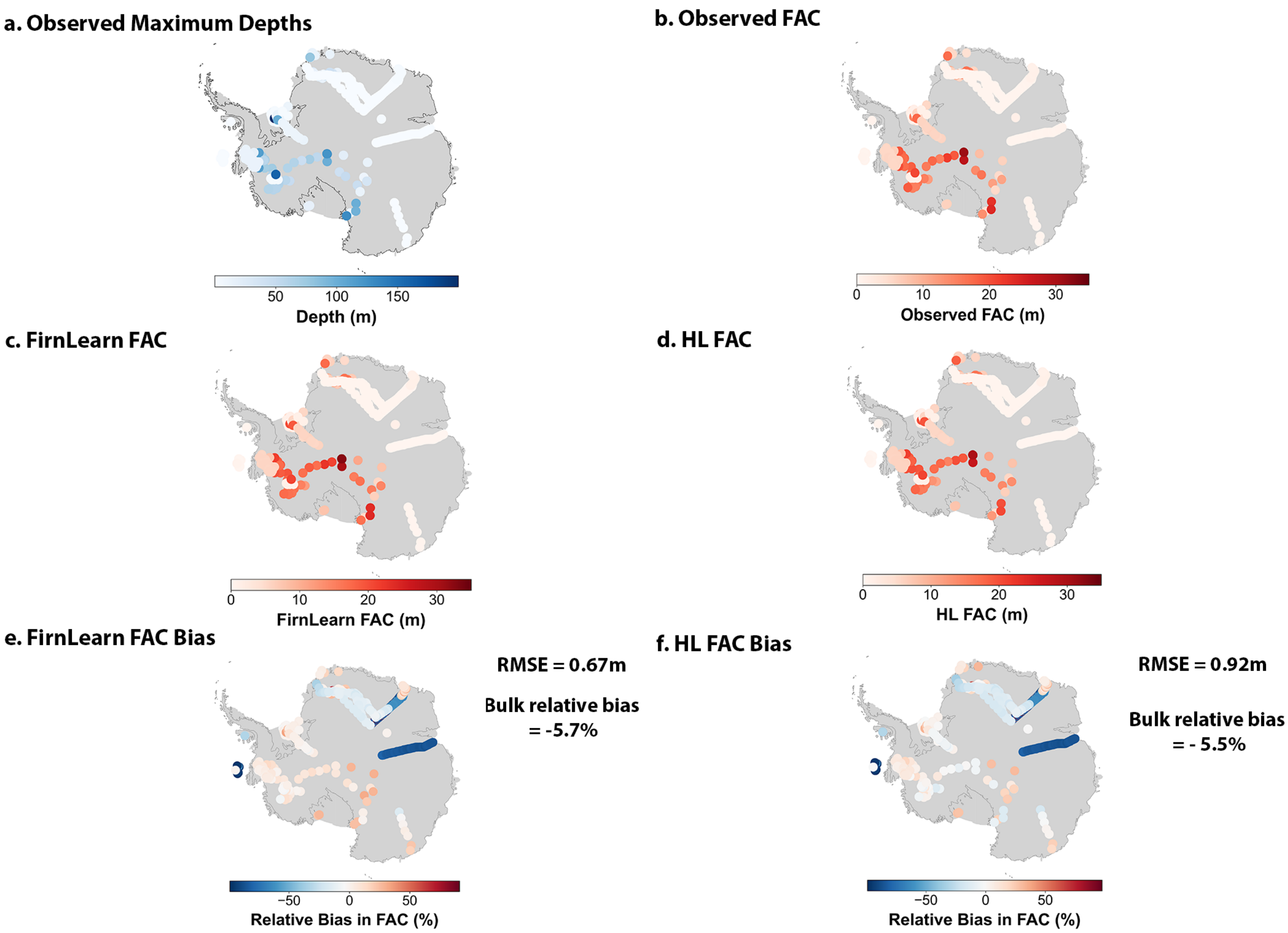

Fig. 6. Firn air content across Antarctica, comparing models to observations and assessing bias: (a) Spatial distribution of 1023 SUMup cores, with shading denoting core depth, (b) Observed FAC from calculated from the densities of the SUMup cores(c) FAC in m, calculated with FirnLearn (d) FAC in m, calculated with Herron and Langway (1980) (e) Relative bias between the FAC calculated with FirnLearn and the observed FAC and (d) Relative bias between the FAC calculated using Herron and Langway (1980) and the observed FAC.

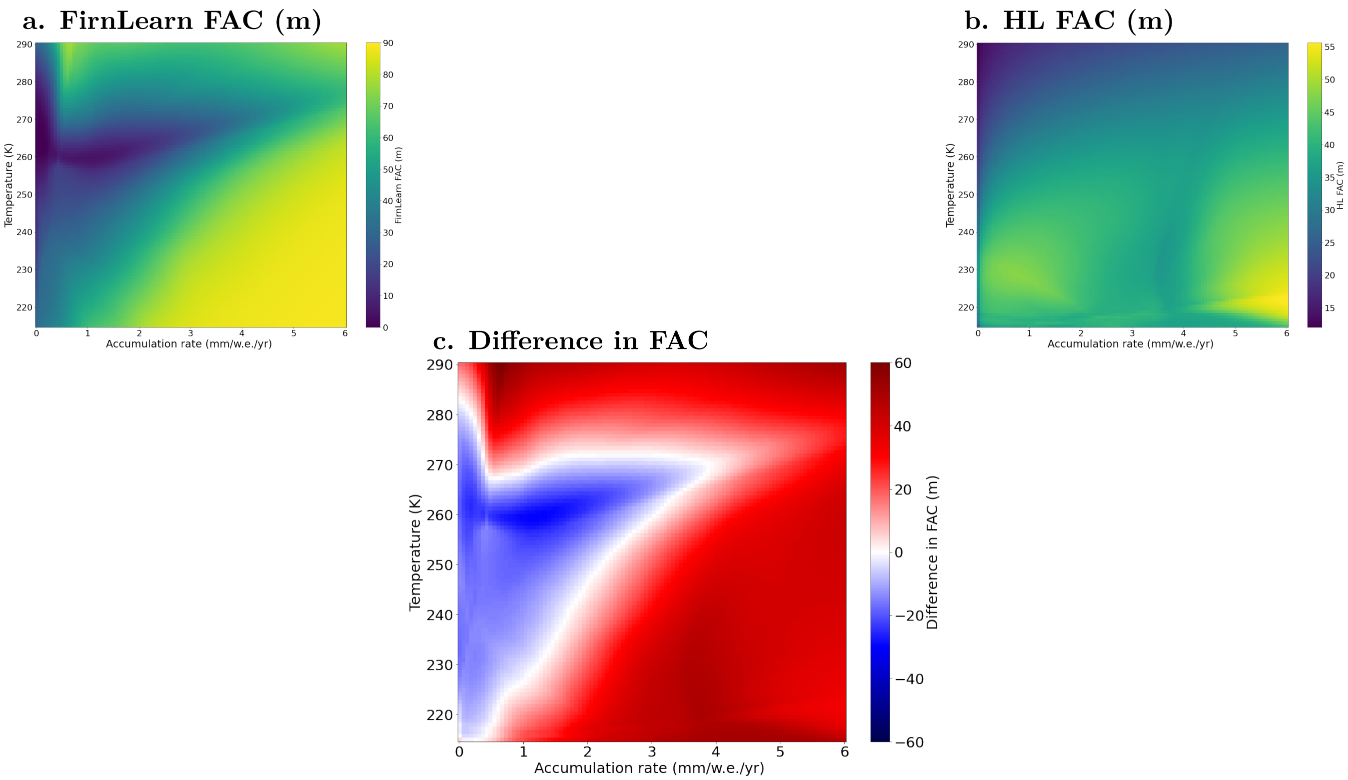

Fig. 7. (a) FAC in m, calculated with FirnLearn, (b) firn air content in meters, calculated with Herron and Langway (1980) (c) Difference in FAC in m, between the FAC calculated using FirnLearn and the FAC calculated using Herron and Langway (1980). The difference is presented as FirnLearn minus HL80. The cluster of black stars indicates the regime of training data regime used for FirnLearn.

with the highest positive differences (FirnLearn $\gg$ Herron and Langway (1980)) are at higher temperatures and higher accumulation rates, as indicated by the red hues. Conversely, the regions with the highest negative differences (FirnLearn $\ll$ Herron and Langway (1980)) are at mid to lower accumulation rates, as indicated by the blue hues, a region which coincides with the parameter space of the training data. It is worth noting that conditions where accumulation rates are very low ($<$ 1 m.w.e. yr $^{-1}$) and temperatures are very high ($>$ 250K [-23°C]) or where accumulation rates are very high ($>$ 4 m.w.e. yr $^{-1}$) and temperatures are very low ($<$ 230K [-43°C]) rarely exist in Antarctica, at least not within its current climate regime. Figure 7 is shown in order to understand FAC values within a wider accumulation rate and temperature parameter space.

LIMITATIONS TO FIRNLEARN

Despite its promising performance, FirnLearn has limitations due to data quality and quantity. As shown in figure 1, the spatial distribution of density observations is notably limited, particularly in East Antarctica. Additionally, as shown in figure 6a, the majority of density observations in the dataset are concentrated at shallow depths. Consequently, the discrepancies between FirnLearn's density predictions and observations increase as depth increases, as evident by the higher RMSE in the predictions of depth at 830 kg m^{-3} compared to the predictions of depth at 550 kg m^{-3} (Fig. 5). Another limitation to FirnLearn is its inability to predict temporal firn density evolution, prompting our adoption of a steady state assumption. Density observations from SUMup are collected over several years, and at different periods of the year, leading to knowledge gaps regarding seasonal variability in firn properties. FirnLearn will struggle to generalize to regions or conditions not represented in the training dataset, potentially leading to biases or inaccuracies in predictions. However, as FirnLearn is trained on more Antarctic firn density data the model will improve. The largest improvements will come from collecting firn density observations at location where (i) there is discrepancy between the HL80 and FirnLearn as well as (ii) where there is poor coverage in accumulation–temperature space, e.g. figure 7(c).

The lack of interpretability of deep learning models like FirnLearn poses challenges. These models are effectively 'black boxes', such that it is difficult to understand the underlying processes governing model predictions. However, given the black-box nature, ANNs serve as effective tools in contexts where predictive accuracy outweighs model interpretability, which is likely the case for depth-density profiles in Antarctica at this time. The improved accuracy offered by ANNs holds the potential to produce improved parameters for understanding firn densification physics.

CONCLUSIONS

In this study, we introduced FirnLearn, a new steady-state densification model for the Antarctic firn layer based on deep learning of data from observations and output from the regional atmospheric climate model. Comparison with observations shows excellent agreement, and comparison to predictions from Herron and Langway (1980) performs comparatively well. In addition, we can use FirnLearn to derive surface density, depth at 550 kg m^{-3} and 830 kg m^{-3} (pore close-off), and firn air content across Antarctica. This study demonstrates the potential of deep learning techniques in improving Antarctic firn density estimates, and strengthens the promising foundation for the development of a generally applicable firn model. In the future, we plan to expand this model by applying it to the Greenland Ice Sheet and coupling it to physics to develop a Physics Informed Neural Network (PINN) which can be applied to both dry and wet firn densification.

DATA AVAILABILITY

FirnLearn's code is available at `https://github.com/ayobamiogunmolasuyi/FirnLearn`. The repository contains all the scripts used to train the models and produce the plots and results. The SUMup dataset is available at `https://github.com/MeganTM/SUMMEDup` while the racmo dataset is here `https://doi.pangaea.de/10.1594/PANGAEA.896940`

SUPPLEMENTAL MATERIAL

The supplement to this article is attached.

ACKNOWLEDGEMENTS

This work was supported by the National Science Foundation (AO, GRFP-2021295396; CRM, 2024132; IB, 1851094), the Army Research Office (CRM, 78811EG), the National Aeronautics and Space Administration (CRM, EPSCoR-80NSSC21M0329). We thank Brice Noel for his assistance in accessing the RACMO data.

REFERENCES

Alley R (1987) Firn densification by grain-boundary sliding: A first model. *Le Journal De Physique Colloques*, **48**(C1) (doi: 10.1051/jphyscol:1987135)

Alley RB (2000) *The two-mile time machine: Ice cores, abrupt climate change, and our future*. Princeton University Press

Anderson D and Benson C (1963) The densification and diagenesis of snow. *MIT Press*

Arnaud L, Barnola JM and Duval P (2000) Physical modeling of the densification of snow/firn and ice in the upper part of polar ice sheets, in: Physics of ice core records. *Hokkaido University Press*

Bader H (1954) Sorge's law of densification of snow on high polar glaciers. *Journal of Glaciology*, **2**

Bader H (1965) Theory of densification of dry, bubbly glacier ice. *US Cold Regions Research and Engineering Laboratory. Research Report 141*

Barnola J, Pimienta P, Raynaud D and YS K (1991) Co2-climate relationship as deduced from the vostok ice core: A re-examination based on new measurements and on a re-evaluation of the air dating. *Tellus B*, **43**(2) (doi: 10.1034/j.1600-3900889.1991.t01-1-00002.x)

Bartelt P and Lehning M (2002) A physical snowpack model for the swiss avalanche warning. *Cold Regions Science and Technology*, **35**(3), 123–145 (doi: 10.1016/s0165-232x(02)00074-5)

Bolibar J, Rabatel A, Gouttevin I, Galiez C, Condom T and Sauquet E (2020) Deep learning applied to glacier evolution modelling. *The Cryosphere*, **14**, 565–584

Brinkerhoff D, Aschwanden A and Fahnestock M (2021) Constraining subglacial processes from surface velocity observations using surrogate-based bayesian inference. *Journal of Glaciology*, **67**(263), 385–403 (doi: 10.1017/jog.2020.112)

Buizer C (2013) Ice core methods | studies of firn air. *Encyclopedia of Quaternary Science*, 361–372

Buizert C, Martinerie P, Petrenko VV, Severinghaus JP, C M Trudinger EW, Rosen JL, Orsi AJ, Rubino M, Etheridge DM, Steele LP, Hogan C, Laube JC, Sturges WT, Levchenko VA, Smith AM, Levin I, Conway TJ, Dlugokencky EJ, Lang PM, Kawamura K, Jenk TM, White JWC, Sowers T, Schwander J and Blunier T (2012) Gas transport in firn: multiple-tracer characterisation and model intercomparison for neem, northern greenland. *Atmospheric Chemistry and Physics*

Burr A, Ballot C, Lhuissier P, Martinerie P, Martin CL and Philip A (2018) Pore morphology of polar firn around closure revealed by x-ray tomography. *The Cryosphere*, **12**(7), 2481–2500 (doi: 10.5194/tc-12-2481-2018)

Camps-Valls G, Reichstein M, Zhu X and Tuia D (2020) Advancing deep learning for earth sciences: From hybrid modeling to interpretability. *IGARSS 2020 - 2020 IEEE International Geoscience and Remote Sensing Symposium* (doi: 10.1109/igarss39084.2020.9323558)

Cuffey KM and Paterson WSB (2010) *The Physics of Glaciers, 4th edition*

Dell RL, Banwell AF, Willis IC, Arnold NS, Halberstadt AR, Chudley TR and Pritchard HD (2022) Supervised classification of slush and ponded water on antarctic ice shelves using landsat 8 imagery – corrigendum. *Journal of Glaciology*, **68**(268), 415–416 (doi: 10.1017/jog.2022.15)

Dunmire D, Banwell AF, Wever N, Lenaerts JT and Datta RT (2021) Contrasting regional variability of buried meltwater extent over 2 years across the greenland ice sheet. *The Cryosphere*, **15**(6), 2983–3005 (doi: 10.5194/tc-15-2983-2021)

Dunmire D, Wever N, Banwell A and Lanearts J (2024) Antarctic-wide ice-shelf firn emulation reveals robust future firn air depletion signal for the antarctic peninsula. *Nature Communications Earth & Environment* (doi: 10.1038/s43247-024-01255-4)

Forster RR, Box JE, van den Broeke MR, Miège C, Burgess EW, van Angelen JH, Lenaerts JT, Koenig LS, Paden J, Lewis C and et al (2013) Extensive liquid meltwater storage in firn within the greenland ice sheet. *Nature Geoscience*, **7**(2), 95–98 (doi: 10.1038/ngeo2043)

Freitag J, Wilhelms F and Kipfstuhl S (2004) Microstructure-dependent densification of polar firn derived from x-ray microtomography. *Journal of Glaciology*, **50**(169), 243–250 (doi: 10.3189/172756504781830123)

Gow AJ (1969) On the rates of growth of grains and crystals in south polar firn. *Journal of Glaciology*, **8**(53), 241–252 (doi: 10.1017/s0022143000031233)

Harper J, Humphrey N, Pfeffer WT, Brown J and Fettweis X (2012) Greenland ice-sheet contribution to sea-level rise buffered by meltwater storage in firn. *Nature*, **491**(7423), 240–243 (doi: 10.1038/nature11566)

Hatie T, R T and J F (2009) *The Elements of Statistical Learning: Data Mining, Inference, and Prediction.* Springer

Helsen MM, van den Brooke MR, van de Wal RS, van de Berg WJ and van Meijgaard E (2008) Elevation changes in antarctica mainly determined by accumulation variability. *Science*, **320**

Herron MM and Langway CC (1980) Firn densification: An empirical model. *Journal of Glaciology*, **25**(93), 373–385 (doi: 10.3189/S0022143000015239)

Kaspers KA, van de Wal RSW, van den Broeke MR, Schwander J, van Lipzig NPM and Brenninkmeijer CAM (2004) Model calculations of the age of firn air across the antarctic continent. *Atmospheric Chemistry and Physics*, **5** (doi: 10.5194/acp-4-1365-2004,2004)

Kingma DP and Ba J (2017) Adam: A method for stochastic optimization

Kipfstuhl S, Faria SH, Azuma N, Freitag J, Hamann I, Kaufmann P, Miller H, Weiler K and Wilhelms F (2009) Evidence of dynamic recrystallization in polar firn. *Journal of Geophysical Research: Solid Earth*, **114**(B5) (doi: 10.1029/2008jb005583)

Li J and Zwally H (2011) Modeling of firn compaction for estimating ice-sheet mass change from observed ice-sheet elevation change. *Annals of Glaciology*, **52**(59) (doi: 10.3189/172756411799096321)

Li W, Veldhuijsen SB and Lhermitte S (2023) Machine learning of antarctic firn density by combining radiometer and scatterometer remote sensing data. *EGUsphere[preprint]* (doi: 10.5194/egusphere-2023-1556)

Li Y and Baker I (2021) Observations of the creep of polar firn. *Journal of Glaciology*, **68**(268), 269–287 (doi: 10.1017/jog.2021.91)

Lightenberg S, Helsen M and den Broeke MV (2011) An improved semi-empirical model for the densification of antarctic firn. *The Cryosphere*, **5**(4)

Ligtenberg SR, Helsen MM and van den Broeke MR (2011) An improved semi-empirical model for the densification of antarctic firn. *The Cryosphere*, **5**(4), 809–819 (doi: 10.5194/tc-5-809-2011)

Lomonaco R, Albert M and Baker I (2011) Microstructural evolution of fine-grained layers through the firn column at summit, greenland. *Journal of Glaciology*, **57**(204), 755–762 (doi: 10.3189/002214311797409730)

LUNDIN JM, STEVENS CM, ARTHERN R, BUIZERT C, ORSI A, LIGTENBERG SR, SIMONSEN SB, CUMMINGS E, ESSERY R, LEAHY W and et al (2017) Firn model intercomparison experiment (firnmice). *Journal of Glaciology*, **63**(239), 401–422 (doi: 10.1017/jog.2016.114)

Maeno N and Ebinuma T (1983) Pressure sintering of ice and its implication to the densification of snow at polar glaciers and ice sheets. *The Journal of Physical Chemistry*, **87**(21), 4103–4110 (doi: 10.1021/j100244a023)

McDowell IE, Albert MR, Lieblappen SA and Keegan KM (2020) Local weather conditions create structural differences between shallow firn columns at summit, greenland and wais divide, antarctica. *Atmosphere*, **11**(12), 1370 (doi: 10.3390/atmos11121370)

Meyer CR and Hewitt IJ (2017) A continuum model for meltwater flow through compacting snow. *Cryosphere*, **11**(6), 2799–2813 (doi: 10.5194/tc-11-2799-2017)

Meyer CR, Keegan KM, Baker I and Hawley RL (2020) A model for french-press experiments of dry snow compaction. *The Cryosphere*, **14**(5), 1449–1458 (doi: 10.5194/tc-14-1449-2020)

Montgomery L, Koenig L, Alexander P and et al (2018) The sumup dataset: Compiled measurements of surface mass balance components over ice sheets and sea ice with analysis over greenland. *Earth Syst. Sci. Data*, **10**(4), 1959–1985

Morris E and Wingham DJ (2014) Densificatio of polar snow: Measurements, modeling, and implications for altimetry. *Jounal of Geophysical Research-Earth Surface*, **119** (doi: 10.1002/2013JF002898)

Noël B, van de Berg WJ, van Wessem JM, van Meijgaard E, van As D, Lenaerts JTM, Lhermitte S, Munneke PK, Smeets CJPP, van Ulft LH, van de Wal RSW and den Broeke MRV (2018) Modelling the climate and surface mass balance of polar ice sheets using racmo2 – part 1: Greenland (1958–2016). *The Cryosphere*

Nussbaumer S, Steiner D and Zumbühl H (2012) Réseau neuronal et fluctuations des glaciers dans les alpes occidentales

Ogunmolasuyi A, Murdza A and Baker I (2023) The onset of recrystallization in polar firn. *Geophysical Research Letters*, **50**(23) (doi: 10.1029/2023gl103435)

O'Shea K and Nash R (2015) An introduction to convolutional neural networks

Reichstein M, Camps-Valls G, Stevens B, Jung M, Denzler J, Carvalhais N and Prabhat (2019) Deep learning and process understanding for data-driven earth system science. *Nature*, **566**(7743), 195–204 (doi: 10.1038/s41586-019-0912-1)

Rizzoli P, Martone M, Rott H and Moreira A (2017) Characterization of snow facies on the greenland ice sheet observed by tandem-x interferometric sar data. *Remote Sensing*, **9**(4), 315 (doi: 10.3390/rs9040315)

Smith B, Fricker HA, Gardner AS, Medley B, Nilsson J, Paolo F, Holschuh N, Adusumilli S, Brunt K, Csatho B, Harbeck K, Markus T, Neumann T, Siegfried MR and Zwally H (2020) Pervasive ice sheet mass loss reflects competing ocean and atmosphere processes. *Science*, **368** (doi: 10.5194/gmd-13-4355-2020)

Steffen K and Box J (2001) Surface climatology of the greenland ice sheet: Greenland climate network. *Journal of Geophysical Research - Atmospheres*, **106**

Steiner D, Walter A and Zumbühl H (2005) The application of a non-linear back-propagation neural network to study the mass balance of grosse aletschgletscher, switzerland. *Journal of Glaciology*, **51**(173), 313–323 (doi: 10.3189/172756505781829421)

Stevens CM, Verjans V, Lundin JM, Kahle EC, Horlings AN, Horlings BI and Waddington ED (2020) The community firn model (cfm) v1.0. *Geoscientific Model Development*, **13**(9), 4355–4377 (doi: 10.5194/gmd-13-4355-2020)

Stevens CM, Lilien DA, Conway H, Fudge TJ, Koutnik MR and Waddington ED (2023) A new model of dry firn-densification constrained by continuous strain measurements near south pole. *Journal of Glaciology*, 1–15 (doi: 10.1017/jog.2023.87)

The-Firn-Symposium-Team (2024) Firn on ice sheets. *Nature Reviews Earth & Environment* (doi: 10.1038/s43017-023-00507-9)

Thompson-Munson M, Wever N, Stevens CM, Lenaerts JT and Medley B (2023) An evaluation of a physics-based firn model and a semi-empirical firn model across the greenland ice sheet (1980–2020). *The Cryosphere*, **17**(5), 2185–2209 (doi: 10.5194/tc-17-2185-2023)

Van den Broeke M (2008) Depth and density of the antarctic firn layer. *J. Neurosci.*, **40**(2), 432–438

van den Broeke M (2008) Depth and density of the antarctic firn layer. *Arctic, Antarctic, and Alpine Research*, **40** (doi: 10.1657/1523-0430(07-021))

Van Wessem J, C R, Morlighem M, Mouginot J, Rignot E, Medley B, Joughin I, Wouters B, Depoorter MA, Bamber JL, Lenaerts JTM, Van De Berg WJ, Van Den Broeke MR and & Van Meijgaard E (2014) Improved representation of east antarctic surface mass balance in a regional atmospheric climate model. *Journal of Glaciology* (doi: 10.3189/2014jog14j051)

Verjans V, Leeson AA, Nemeth C, Stevens CM, Kuipers Munneke P, Noël B and van Wessem JM (2020) Bayesian calibration of firn densification models. *The Cryosphere*, **14**(9), 3017–3032 (doi: 10.5194/tc-14-3017-2020)

Supporting Information for

FirnLearn: A Neural Network based approach to Firn Densification Modeling for Antarctica

Ogunmolasuyi et al.

Correspondence to: Ayobami Ogunmolasuyi (ayobami.o.ogunmolasuyi.th@dartmouth.edu)

1. Supplemental models

a. The Elastic net linear regression model:

The Elastic Net (Zou & Hastie, 2005) is a least squares linear regression method that combines the strengths of the ridge regression (Hoel & Kennard, 1970) and the Lasso regression (Tibshirani, 1996) for improved regularization. Lasso creates a simpler and more interpretable model by adding a regularization term to the cost function of the standard linear regression by selecting a subset of the features (Hastie et al., 2009). This regularization term constrains the size of the estimated coefficients by shrinking coefficients or setting them to zero. Ridge, on the other hand, addresses the multicollinearity of the standard linear regression model by adding a penalty term which shrinks the coefficients. Both Lasso and Ridge regression are also regularization methods used to reduce overfitting. Lasso also called L1 regularization adds the sum of the squares of the regression parameters to the objective function while Ridge, also called L2 regularization adds the sum of the squares of the regression parameters. ElasticNet is expressed as follows:

The hyperparameters in the ElasticNet regression are α, the constant that multiplies the penalty terms, the l1 ratio, which is the ElasticNet mixing parameter, ranging from 0, making the penalty an L2 penaty, to 1, making the penalty an L1 penalty. Hyperparameter tuning with GridSearchCV yields the following result:

Parameters	Hyperparameter range	Best performing hyperparameter
α	0.001,0.01,0.1,1	0.01
L1 ratio	0.1,0.2,0.5,0.7,0.9,1	1

Table S1: Hyperparameter range and selected optimal values for the elastic net model

The best performing L1 ratio of 1in the table above indicates that Lasso produces the better linear model.

b. The random forest model

This is an ensemble method that builds multiple decision trees during training and averages their result to get a more accurate and stable output (Breiman, 2001). The Random Forest model builds these different trees independently and in parallel.

The hyperparameters tuned in this Random Forest model are the number of trees in the forest, the maximum depth of the tree, the minimum number of samples required to split a node. Hyperparameter tuning with GridSearchCV yields the following result:

Parameters	Hyperparameter range	Best performing hyperparameter
number of trees	50,100,200,300	300
maximum depth of the tree	None, 2, 4, 6, 10	1
Minimum number of samples to split a node	1,2,5,9,10	10

Table S2: Hyperparameter range and selected optimal values for the random forest model

c. The gradient boosting model

Like the Random Forest model, the Gradient Boosting model is an ensemble method that combines the results of different trees. However, the trees in Gradient Boosting are built sequentially, with each new tree being trained to correct the errors made by the preceding tree.

The hyperparameters tuned in this Gradient Boosting regression model are the number of trees in the forest, the maximum depth of the tree, the minimum number of samples required to split a node, the minimum number of samples required to be at a leaf node. Hyperparameter tuning with GridSearchCV yields the following result:

Parameters	Hyperparameter range	Best performing hyperparameter
number of trees	25, 50,100,200	50
maximum depth of the tree	None, 2, 4, 6, 10	1
Minimum number of samples to split a node	2 ,5,9,10	10
Learning Rate	0.01,0.1,0.5	0.5

Table S3: Hyperparameter range and selected optimal values for the gradient boosting model

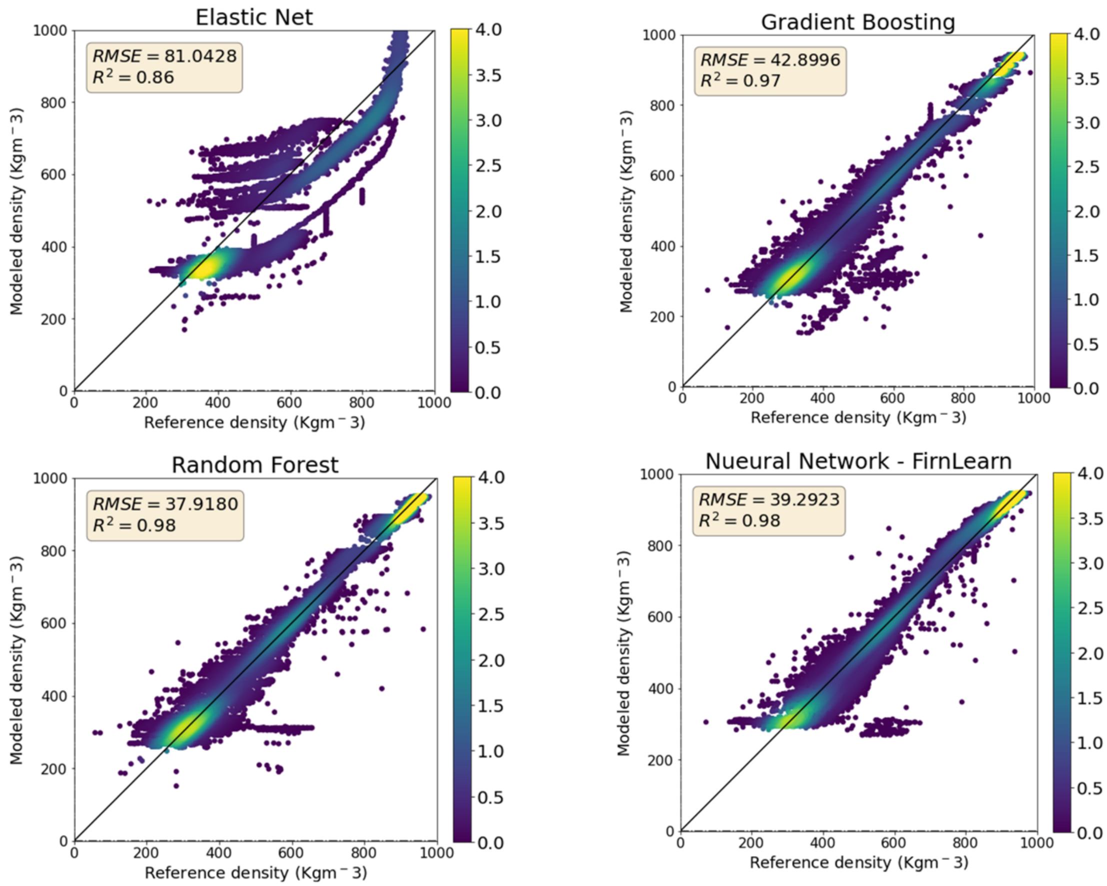

Figure S1: Comparison of modeled density against ground truth density for the (a) Elastic Net model (b) Gradient Boosting model (c) Random Forest regressor and (d) Neural network model – FirnLearn, obtained using cross-validation. The color range blue-yellow indicate the density of the points, used to visualize areas of higher concentration of data points.

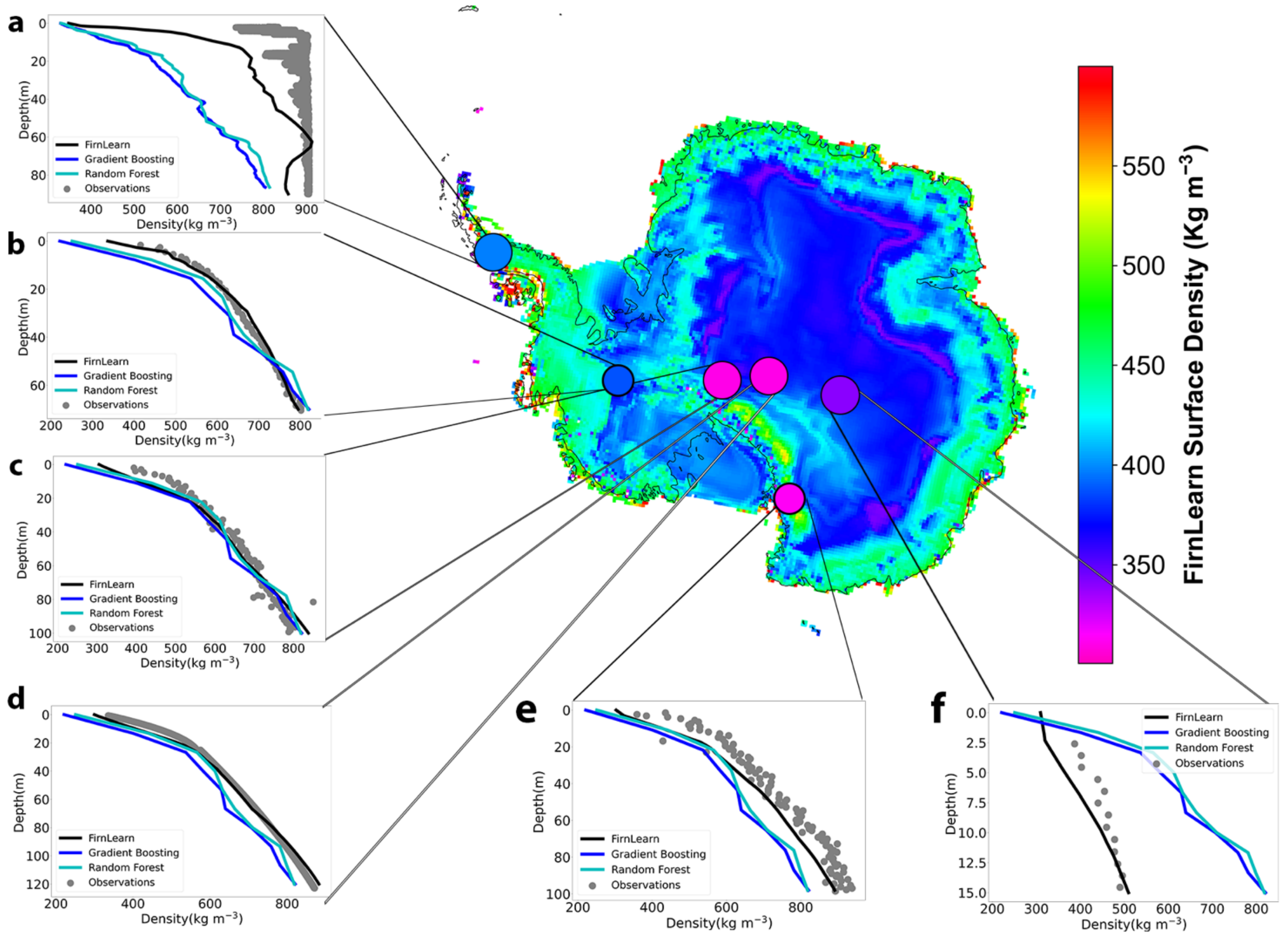

Figure S2. Depth-density profiles at the 6 test sites. Shown corresponding to each site are the observed density profiles (ground truth) in grey, the FirnLearn modeled profile in black, the random gradient boosting model in blue, and the random forest model in cyan for (a) a location on the Larsen C Ice Shelf, (b) location on the Marie Byrd Land, (c) location near the South Pole,(d) the South Pole, (e) the Taylor dome, and (f) a location near Vostok station.

As shown in Figure S1, the Random Forest and Neural Network (FirnLearn) models are the best-performing models, both with an R^2 score of 0.97. The Random Forest model has a 5% lower RMSE than the neural Network, suggesting that it might have a slight edge in predictive accuracy. To evaluate the better performing model, we tested the models on the six test sites in Figure 3.

As shown in Figure S2, for all sites, while the performance of these models are very comparable, FirnLearn generally provides a more accurate and smoother prediction of depth-density profiles compared to the random forest and gradient boosting models.

References

Breiman, L. Random Forests. *Machine Learning* **45**, 5–32 (2001). https://doi.org/10.1023/A:1010933404324

Hastie, T., Friedman, J., & Tibshirani, R. (2022). Elements of statistical inference. *Principles of Statistical Analysis*, 161–162. https://doi.org/10.1017/9781108779197.016

Hoerl, A. E., & Kennard, R. W. (2000). Ridge regression: Biased estimation for nonorthogonal problems. *Technometrics*, *42*(1), 80. https://doi.org/10.2307/1271436

Tibshirani, R. (2011). Regression shrinkage and selection via the Lasso: A retrospective. *Journal of the Royal Statistical Society Series B: Statistical Methodology*, *73*(3), 273–282. https://doi.org/10.1111/j.1467-9868.2011.00771.x

Zou, H., & Hastie, T. (2005). Regularization and variable selection via the elastic net. *Journal of the Royal Statistical Society Series B: Statistical Methodology*, *67*(2), 301–320. https://doi.org/10.1111/j.1467-9868.2005.00503.x